

On the oxidation and ignition of uranium carbide fragments in air and comparison with zirconium carbide oxidation

Gasparri, C.; Podor, R.; Fiquet, O.; Rushton, M.J.D.; Lee, W.E.

Journal of Nuclear Materials

DOI:

[10.1016/j.jnucmat.2024.154944](https://doi.org/10.1016/j.jnucmat.2024.154944)

Published: 15/04/2024

Publisher's PDF, also known as Version of record

[Cyswllt i'r cyhoeddiad / Link to publication](#)

Dyfyniad o'r fersiwn a gyhoeddwyd / Citation for published version (APA):

Gasparri, C., Podor, R., Fiquet, O., Rushton, M. J. D., & Lee, W. E. (2024). On the oxidation and ignition of uranium carbide fragments in air and comparison with zirconium carbide oxidation. *Journal of Nuclear Materials*, 592, Article 154944.
<https://doi.org/10.1016/j.jnucmat.2024.154944>

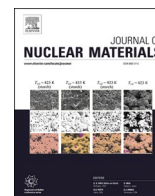
Hawliau Cyffredinol / General rights

Copyright and moral rights for the publications made accessible in the public portal are retained by the authors and/or other copyright owners and it is a condition of accessing publications that users recognise and abide by the legal requirements associated with these rights.

- Users may download and print one copy of any publication from the public portal for the purpose of private study or research.
- You may not further distribute the material or use it for any profit-making activity or commercial gain
- You may freely distribute the URL identifying the publication in the public portal ?

Take down policy

If you believe that this document breaches copyright please contact us providing details, and we will remove access to the work immediately and investigate your claim.



On the oxidation and ignition of uranium carbide fragments in air and comparison with zirconium carbide oxidation

C. Gasparrini^{a,1,*}, R. Podor^b, O. Fiquet^c, M.J.D. Rushton^{a,d}, W.E. Lee^{a,d}

^a Department of Materials & Centre for Nuclear Engineering, Imperial College London, London SW7 2AZ, United Kingdom

^b ICSM, University Montpellier, CNRS, CEA, ENSCM, Site de Marcoule, Bagnols sur Ceze, France

^c CEA, DES, IRESNE, DEC, SA3E, LCU, CEA Cadarache, Saint-Paul-Lez-Durance F-13108, France

^d Nuclear Futures Institute, Bangor University, Dean Street, Bangor LL57 1 UT, Gwynedd, United Kingdom

ARTICLE INFO

Keywords:

Uranium carbide
Zirconium carbide
Ignition
Pyrophoricity
Oxidation

ABSTRACT

Oxidation of uranium carbide (UC) small fragments from sintered pellets was experimentally tested to better understand UC safe-handling procedures given the renewed interest of non-oxide fuels for high temperature gas or liquid metal cooled reactors. Transformation from UC to U_3O_8 via a self-ignition reaction was observed at partial pressure of oxygen as low as 10 Pa. The heat output from UC self-ignition in fragments (not-free from UO_2 contamination) previously stored in either air atmosphere or inert-atmosphere during a three months period was monitored at 973 K and 1073 K in air atmosphere in a TGA/DTA and no difference could be observed. Residual carbon content, measured as amorphous carbon, carbide or CO/CO_2 , decreased with exposition temperature in U_3O_8 resulting oxide, this is in contrast with zirconium carbide resulting oxide, ZrO_2 . Cracking and stresses accumulated in the oxide were highest for UC to U_3O_8 compared to UC to UO_2 reactions and ZrC to ZrO_2 reactions.

1. Introduction

Advanced technology fuel (ATF) [1–3] describes a class of non-oxide nuclear fuels under reconsideration for applications in non-water cooled reactors. These fuels have higher thermal conductivity [4] than oxide fuels (UO_2) and improved fuel performance [5] during operation thanks to their higher fissile density and better compatibility with gases or liquid metal coolants [6]. The alternative fuels under consideration includes uranium carbides, nitrides, silicides and a combination of these [7–10]. Uranium carbides, nitrides and silicides were considered in the past for application in liquid metal reactors, high temperature gas reactors and nuclear space propulsion systems [11]. They are currently being re-evaluated and are considered essential for the development of sodium fast reactor programs [12].

This work focuses on uranium carbide (UC) sintered fragments and the assessment of their reactivity in oxygen/air atmosphere tested for safe handling during storage and for conversion into an oxide form prior to the reprocessing stage or permanent disposal when considered waste. ATFs were widely studied in the 1950s and 60s when they were tested in

research reactors. In the UK, a large legacy of ATFs were stored for decades awaiting for conditioning treatment prior to their final disposal [13].

ATFs offer benefits during operation given their higher fuel density and thermal conductivity that inhibit overheating, however, their main drawback is that they need extra requirements during manufacturing and a careful handling throughout the fuel cycle when compared to oxide fuels to inhibit their reactivity to oxygen and air exposure [14]. The extra precautions during manufacturing and handling rely on the fact that unwanted oxygen entering as a contaminant during manufacturing can deteriorate their properties [6,14]. Additionally, exposure to air atmosphere during fuel handling may be hazardous given the pyrophoric nature of ATFs when in powder form [15,16] and there is limited experience compared to oxide fuels. For safe disposal, conversion into a suitable oxide form is often considered as a necessary step. This is confirmed by the UK's Nuclear Decommissioning Authority (NDA) decision that all carbides and mixed carbides legacy fuels in the UK [17,13] need to be fully oxidised prior to final disposal. This conditioning treatment relies on complete and full oxidation. Oxidation is

* Corresponding author.

E-mail addresses: cg1614@ic.ac.uk, claudia.gasparrini@jensenhughes.com (C. Gasparrini).

¹ Current address: Jensen Hughes, Via Keplero 5, 20016 Pero, Milan, Italy.

not a straightforward process for this family of materials given the tendency for carbides, as well as nitrides [15,18] and silicides [19,20], to self-ignite when exposed to oxygen and/or steam releasing a large amount of heat [15] depending on temperature and oxygen atmosphere. Unwanted oxidation reactions can also occur during reactor operation (in an accident scenario), so it is important to better understand fuel ignition and oxidation. The mechanism of self-ignition reported in this work for UC is also shared with other ATFs [15,21]. UC reactivity and self-ignition mechanism was investigated and compared with past [15] and recent studies [16,22–24]. In this work, UC fragments were exposed to air at temperature after being stored in either air or inert atmospheres to compare the heat release. Ignition can be generally studied using isothermal tests or burning curve tests [25]. In this work we have applied both methodologies. The novelty of what is presented is in the use of novel and advanced characterisation techniques such as high temperature environmental scanning electron microscopy (HT-ESEM) and thermogravimetric analysis coupled with differential thermal analysis (TGA/DTA) or mass spectrometry (TGA-MS) to enable an in depth understanding of the mechanism and visual characterisation of the self-ignition process triggered at low partial pressures of oxygen on sintered fragments produced from dense pellets of UC.

Another carbide material that shares common challenges and opportunities with ATFs fuels is ZrC. This is being considered for use as an ATF cladding in tri-structural isotropic-coated (TRISO) fuel particles to replace SiC thanks to its high melting temperature, above 3500 K, low neutron absorption cross section and good resistance to fission products corrosion [26]. ZrC, like UC, requires special requirements during manufacturing to ensure the right stoichiometry and avoid oxygen contamination [27]. The combination in a fuel architecture where both UC and ZrC are considered is the development of nuclear thermal propulsion reactors by NASA [11,28]. The similarities and differences in the behaviour of these two materials will be the basis for the discussion in this work. One of the main improvements in the understanding of the initiation of the ignition process was related to oxide cracking. In ZrC, cracking governed the rate of the reaction and the formation of a characteristic Maltese cross shape in the resulting ZrO_2 oxide [29]. This shape has also been reported for UC [30] and other carbides and nitrides or metals from the IV, V and VI groups of the transition metals [31,32]. In UC, exponentially driven crack networking, caused by a sample fragmentation process was linked to ignition initiation [23]. The influence of temperature was also found to be key in both ZrC and UC oxidation, as it affected not only the oxide morphology and its protectiveness but also in the reactivity of carbon with oxygen [24]. This is particularly important within the nuclear industry as there is a need to discriminate between residual unreacted carbon and unreacted carbide within the oxide. In this work, the similarities in the behaviour of these two carbides: ZrC and UC when exposed to oxygen environment will be discussed.

2. Experimental details

UC self-ignition mechanism was tested on fragments exposed to oxygen or air atmospheres in TGA-DTA or in a HT-ESEM. Two batches of samples were tested

- Samples produced from UC pellets that were previously stored in air atmosphere for decades, these were legacy fuels from the Dounreay site, Scotland, U.K. These pellets, together with other ‘uranics’, were produced from fuel cycle operations since the 1950’s and stored at the Dounreay site [33].
- Samples produced from UC pellets manufactured and stored in gloveboxes in inert argon atmosphere (continuously purified < 5 ppm O_2) at CEA Cadarache, France. Samples were stored in tight metallic canisters inerted with argon. These pellets were manufactured in mid 2014 and the age between manufacturing and testing in this work was approximately 2 years.

2.1. UC samples stored in air, Dounreay legacy fuel

The reactivity of UC fragments coming from Dounreay legacy fuels was studied by testing and comparing freshly made fragments kept in an inert atmosphere, inside a glovebox with fragments stored in air atmosphere, in a fume-hood, for three-months. The comparison was achieved by comparing the heat released during ignition on the two set of samples. The following approach was used: cylindrical pellets were selected from the same batch. After selection, a few pellets were placed inside an inert glovebox, while other pellets were stored in a fume-hood. These pellets were then crushed with a hammer to obtain small fragments (each with mass approximately ≤ 70 mg). This was performed inside the glovebox to produce inert-stored fragments (“freshly made fragments” as labelled at the beginning of this paragraph), or in the fume hood to produce air-stored fragments. UC samples in the form of fragments were taken from the middle of each crushed pellet to make sure oxygen contamination coming from UC outer layer being exposed for decades in air was kept to a minimum. These were labelled:

- air-stored: fragments obtained by crushing UC pellets in air (sparks visible during crushing)
- inert-stored: fragments obtained by crushing UC pellets inside a glovebox (no sparks detected during crushing thanks to the inert atmosphere)

Fragments were used to study UC reactivity using TGA/DTA analysis in isotherm mode. UC fragments, in the range of 15–65 mg in mass, were inserted in a TGA/DTA Netzsch 449C STA (Netzsch Group, Germany) where oxidation and ignition reactions were monitored. The crucibles used for all experiments were alumina sample crucible type GB445213 (3.4 ml). Samples inserted in the TGA/DTA were first exposed to an isotherm at room temperature in argon gas, set at 200 ml/min, to purge the TGA/DTA chamber and limit oxygen contamination. An isotherm in argon at room temperature was performed to avoid residual oxygen that could affect UC reactivity, when possible the isotherm was performed for 14 h (overnight), otherwise it was performed for 3 h. Results used and reported for this work are the ones where no active oxidation was observed during the isotherm in argon (the mass profile was flat and stable). Purging in argon for hours was found to be a necessary step as UC samples were highly reactive and they oxidised during the heating ramp in argon if the chamber was not completely purged beforehand. The purity of argon used was 99.998 %, piping were in stainless steel and copper or plastic, no oxygen scrubber was present. The TGA/DTA was not located inside an inert glovebox, hence, some oxygen contamination during sample transfer cannot be completely ruled out but it was minimised by sealing UC inert-stored fragments in a metallic holder filled with inert gas during sample transfer. After the isotherm in argon at room temperature, heating was performed at a rate of 50 K/min under argon flow (200 ml/min) to the desired temperature (either 973 K or 1073 K). When the temperature was reached, the sample was kept on hold for 20 min in argon to allow temperature stabilisation before switching the atmosphere to air. The air flow for the oxidation experiment was set to 60 ml/min, to be consistent with ZrC TGA oxidation experiments. The heat output results are reported in $\mu\text{W}/\text{mg}$ since the Equipment was a TGA/DTA.

Ignition experiments in burning curve mode in a TGA/DTA were performed by heating the samples from room temperature to 1673 K with a heating rate of 10 K/min. The samples will be referred to as Sample A (mass= 63.9 mg), B (mass= 15.6 mg) and C (mass= 20.5 mg). After these experiments, UC fragments and oxide powders were characterised using an X’Pert 3 powder diffractometer (PANalytical, The Netherlands) with Ni-filtered $\text{CuK}\alpha$ radiation. Samples were scanned from $2\theta=10^\circ$ to 75° . Identification of phases from XRD patterns was performed using the International Centre for Diffraction Data (ICDD) database by comparing peak positions in the experimental patterns with those previously tabulated for relevant compounds and listed in the

Powder Diffraction Files (PDF). Secondary electron images (SEIs) on UC samples and oxidised U_3O_8 powders were acquired with a FEI Quanta 200 FEG (Thermo Fisher Scientific, Massachusetts, USA).

2.2. UC samples produced in glove box, CEA Cadarache

High temperature environmental SEM (HT-ESEM) experiments were performed using a FEI Quanta 200 FEG ESEM [23,24]. UC discs samples were stored in an inert glovebox (Ar gas) after being manufactured in gloveboxes in inert argon atmosphere (continuously purified < 5 ppm O_2). Details related to samples manufacturing procedure can be found in G. Raveau work [34]. To produce fragments for the experiments here presented, discs were broken in the glove box and fragments were transferred in a closed Teflon box. This Teflon box was opened in air whilst fragments were transferred to the ESEM chamber as quickly as possible. UC fragments were exposed to air in the ESEM laboratory where samples were weighed prior to insertion in the SEM chamber. Then, SEM chamber was pumped to high vacuum (10^{-3} Pa) within 2 min. No apparent surface oxidation was observed on the fragments at the micrometer scale when monitored with secondary electron images (SEIs). Samples were heated with a rate of 20 K/min with a partial pressure of either 100 Pa O_2 or 10 Pa O_2 , fragments mass ranged between 12 and 33 mg.

Photographs showing the shape and appearance of samples from Dounreay legacy fuels and CEA Cadarache is shown in Fig. 1. Since it was not possible to manufacture samples with fixed geometry from these pellets, fragments tested were chosen to be of similar shape and mass.

2.3. ZrC samples

Oxidation of ZrC sample, manufactured via hot pressing, were tested in isotherm mode in a TGA/DTA Netzsch STA 449F1 (Netzsch Group, Germany) at 1073, 1173, 1273 and 1373 K. The manufacturing and

characterisation of ZrC samples is reported in [29,35]. As shown in Gasparrini et al. [27], carbon, oxygen and nitrogen contaminations were detected in these samples by elemental analysis. It was demonstrated that to clearly define stoichiometry in ZrC_x , multiple techniques should be used together [27]. Samples were first exposed to an inert, argon atmosphere using a 60 ml/min flow rate as the sample was heated from room temperature at a rate of 10 K/min to compare the results with UC experiments. When the desired temperature was reached, argon flow was maintained for approximately 15 min to allow temperature stabilisation before an air atmosphere was introduced at a flow rate of 60 ml/min.

3. Results

Ignition of UC is known to be affected by several factors [15], here a relationship between oxygen partial pressure and temperature was investigated on UC fragments stored in air or stored in inert atmosphere.

Characterisation of air-stored or inert-stored UC fragments produced by crushing legacy fuels from Dounreay was performed by XRD as shown in Fig. 2. Uranium carbide and oxide phases in the samples were labelled against PDF data files: UC [36], U_2C_3 [37] and UO_2 [38], cubic phases.

XRD analysis in Fig. 2 revealed that fragments from UC sintered pellets (Dounreay legacy fuels) crushed in air atmosphere or inert atmosphere both contained a UO_2 phase. The inert-stored sample XRD pattern was taken with a specially designed holder that isolated the specimens from air atmosphere. Given the use of the specially designed older, and since no sparks were detected during crushing of the pellet in the glove-box, it is plausible that UO_2 may have already been present in the pellet prior to crushing in inert atmosphere.

UC reactivity was assessed considering the exposure to air or inert atmospheres. The inert-stored and air-stored fragments reactivity was quantified by measuring the heat released during controlled isothermal

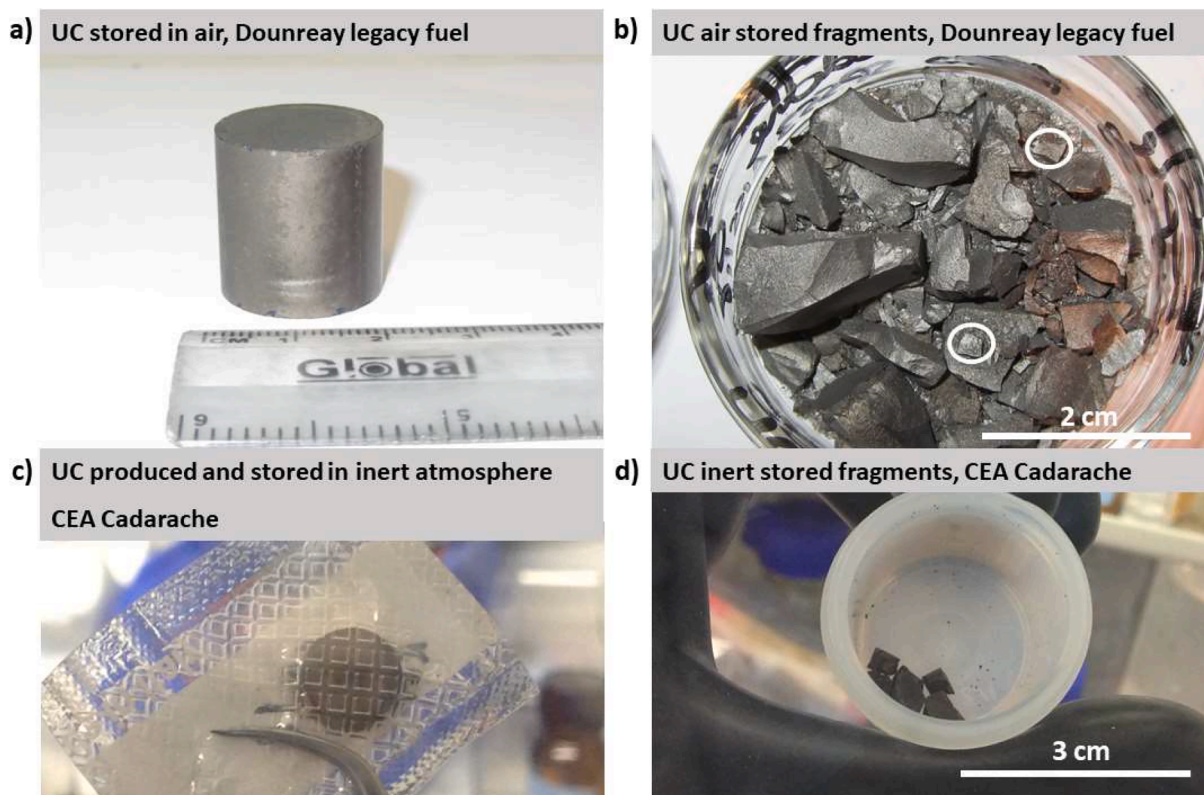


Fig. 1. Photographs of a) Dounreay legacy fuel pellets and b) type of fragments chosen to be tested in TGA experiments; c) CEA Cadarache pellet and d) type of fragments chosen to be tested in HT-ESEM.

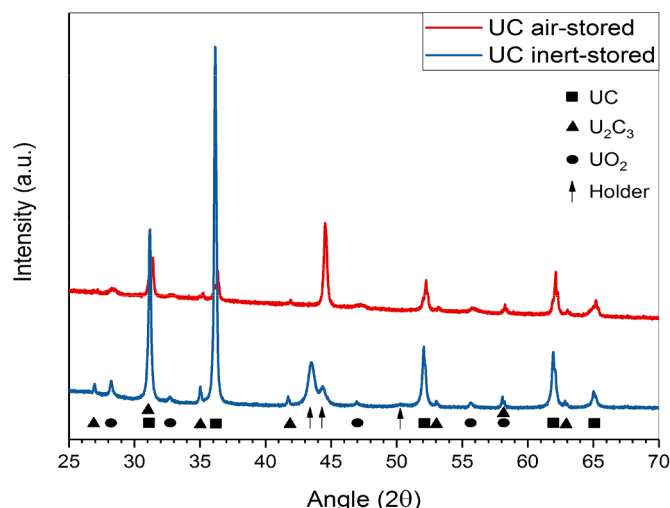


Fig. 2. XRD characterisation of UC fragments which were crushed and kept in air atmosphere (air-stored) or in inert atmosphere (inert-stored), from Dounreay legacy fuels. Peaks were identified against PDF 01 073 1709 [36] for UC, PDF 01 074 0805 [37] for U_2C_3 , and PDF 00 041 1422 for UO_2 [38].

oxidations in a TGA/DTA under the same conditions of temperature and oxygen pressure. The inert-stored samples were transferred to the TGA/DTA room from the glovebox sealed in a metallic holder in order to keep UC fragments in an inert atmosphere for as long as possible. Fig. 3 shows a schematic of the test used, the increase in mass change in the 93rd minute is due to the adjustment of the argon flow from 200 ml/min to 60 ml/min (see experimental details).

The area highlighted under the DTA peak shown in Fig. 3 represents the heat output measured from oxidation experiments. Comparison between air-stored and inert-stored heat output values is given in Table 1. The tests were performed over a period of three months with air-stored samples kept always in air and inert-stored samples kept always inside the glovebox.

As shown in Table 1, the heat output from inert-stored and air-stored fragments was the same considering the error bars indicating that storage of UC samples (Dounreay legacy fuels) in air did not affect their reactivity, as no quantifiable change in reactivity was measured. These results suggest that these UC samples, in the form of pellets or solid fragments, could be handled in air without affecting oxidation or

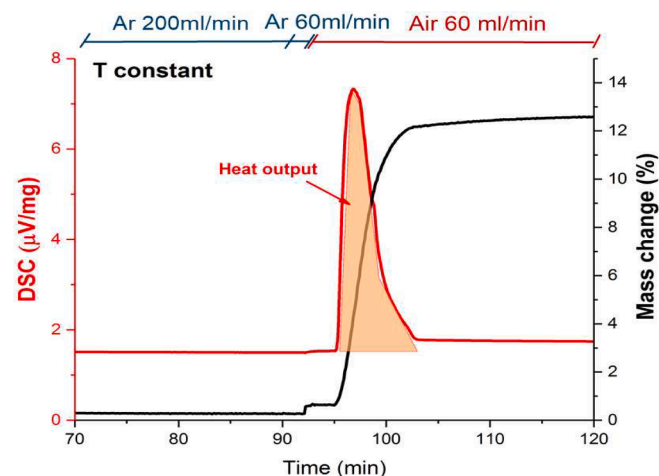


Fig. 3. TGA/DTA run performed on air-stored and inert-stored fragments, this is a representative curve since both experimental conditions showed the same profile. The area highlighted under the DTA peak represents the heat output evaluated in $\mu V/mg$.

Table 1

Heat output released from isothermal oxidation performed in a TGA/DTA from air-stored and inert-stored fragments.

T (K)	Air-stored Heat output ($\mu V/mg$)	Inert-stored Heat output ($\mu V/mg$)
973	1460 ± 135	1464
1073	1149 ± 10	1178 ± 31

ignition results. This was an important consideration in planning the experiments, as using gloveboxes introduces additional complexity in comparison of using fume-hoods. The outcome of this research was considered representative of the behaviour of all UC Dounreay legacy fuel samples used in this study, hence, air handling was conducted in further experiments [24].

Ignition of UC fragments in burning curve experiments (thermal ramp) was investigated using TGA-DSC and *ex situ* characterisation with a SEM. UC ignition was monitored from the heat release, the peak in the temperature profile and by observing the morphology of the oxide samples *ex situ*. Fig. 4 exhibits three distinct behaviours during UC oxidation: Sample A experienced gradual oxidation, Sample B underwent ignition while Sample C underwent rapid ignition. All these samples were completely oxidised to U_3O_8 , as confirmed by XRD analysis. The total mass increase of approximately 12 % was found to correspond to complete conversion of UC to U_3O_8 [24]. The TGA/DSC data obtained are shown in Fig. 4. According to Dell and Wheeler [15] one of the main factors affecting initiation and propagation of UC during oxidation is linked to specimens mass and geometry, this was tested in this work as can be seen by results shown in Fig. 3 where experimental set up was the same, but the size of specimens was different.

The gradual oxidation of Sample A was characterised by a broad heat flow profile and no increase in the temperature of the sample holder (compare Fig. 4a and d). Samples that underwent ignition, B and C, presented a sharp increase in mass (see Fig. 4b and c). The sharp increase in mass was accompanied by a sharp heat release and a sharp increase in the temperature of the sample holder (see Fig. 4d). UC ignition is accompanied by a large amount of heat release as it proceeds as a highly exothermic reaction, with a reported $\Delta_r H^0 = -1487.21$ kJ/mol at 298.15 K [15]. Reaction considered is:



As a result of the large heat release, a sharp temperature increase follows and this is reported in the temperature profiles of the TGA sample holder (see Fig. 4d) on samples that underwent ignition (Samples B and C). The temperature at which the ignition process started is shown in Fig. 5a where mass gain is plotted against time and temperature. Fig. 5b shows the overall sample holder temperature increase detected in samples B and C by subtracting the measured temperature of the system from the nominally programmed temperature.

The ignition temperature was determined to be approximately 683 K for sample C and 698 K for sample B. The sample crucible temperature increase during ignition ranged between 30 K and 35 K. *Ex situ* analysis by XRD confirmed the product of ignition to be U_3O_8 . Observation of the oxide morphology was performed by SEM both on samples that had undergone ignition (sample C) and those that had not (sample A). The difference in the oxide morphology produced by oxidation or ignition is shown in Fig. 6. Fig. 6a and b showed backscattered electron images (BSEI) of the non-ignited sample (A) revealing a compact structure of the oxide with neck growth between rounded particles inferring the initiation of a natural sintering process. The morphology of the ignited sample, instead, showed a disrupted oxide (see Fig. 6e). It displayed rounded particles that were not interconnected as if the sample burst (compare Fig. 6b and f).

Burning curve tests were conducted on UC fragments in a controlled atmosphere (at different partial pressures of oxygen) in a HT-ESEM and in a TGA/DSC (using compressed air). Ignition was monitored either

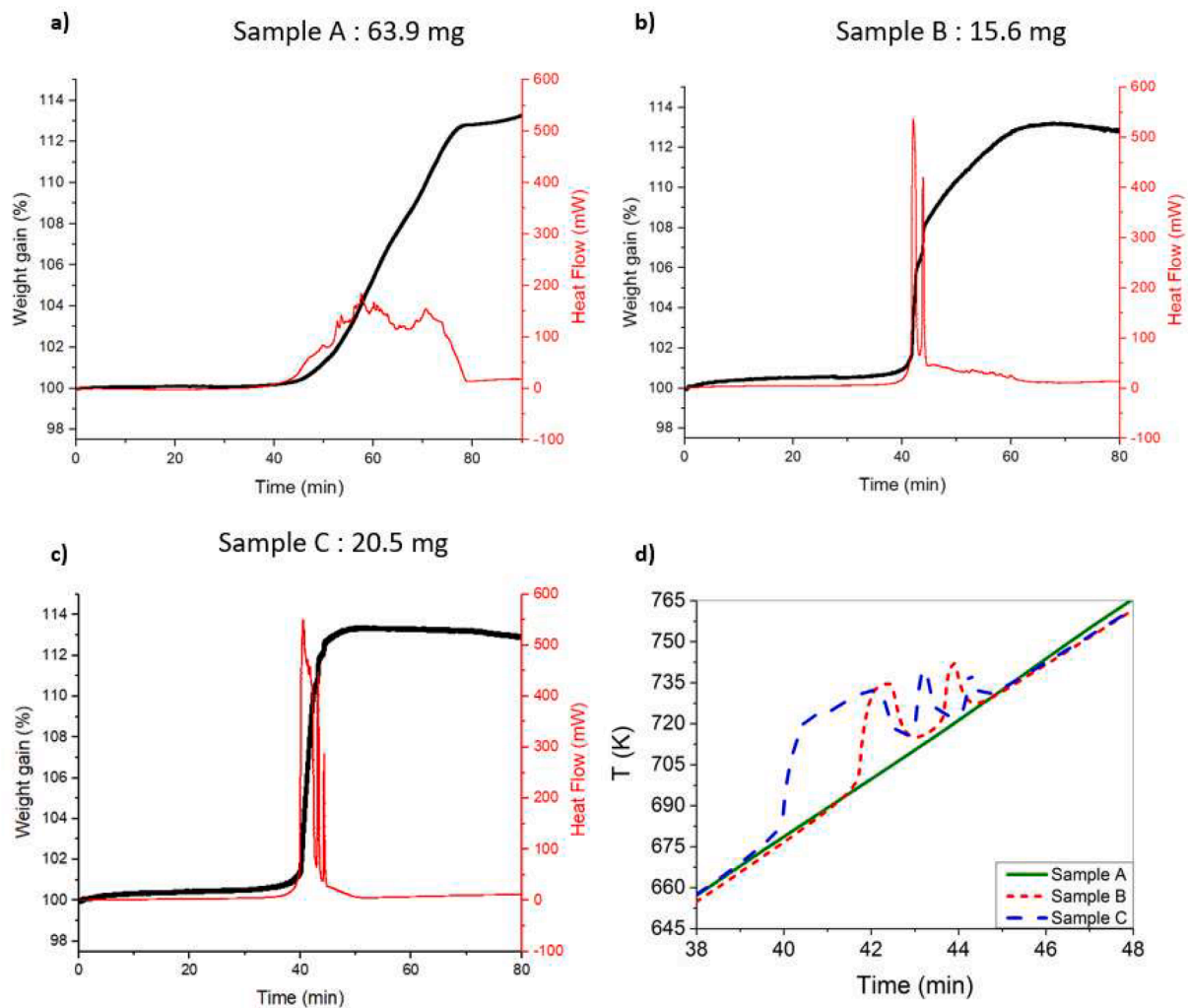


Fig. 4. TGA/DSC signals during UC oxidation from 298 –1673 K in air a) gradual oxidation (Sample A), b) ignition (Sample B), c) rapid ignition (Sample C), d) sample holder temperature profile of samples A, B and C: crucible overheated due to self-ignition mechanism in Sample B and C.

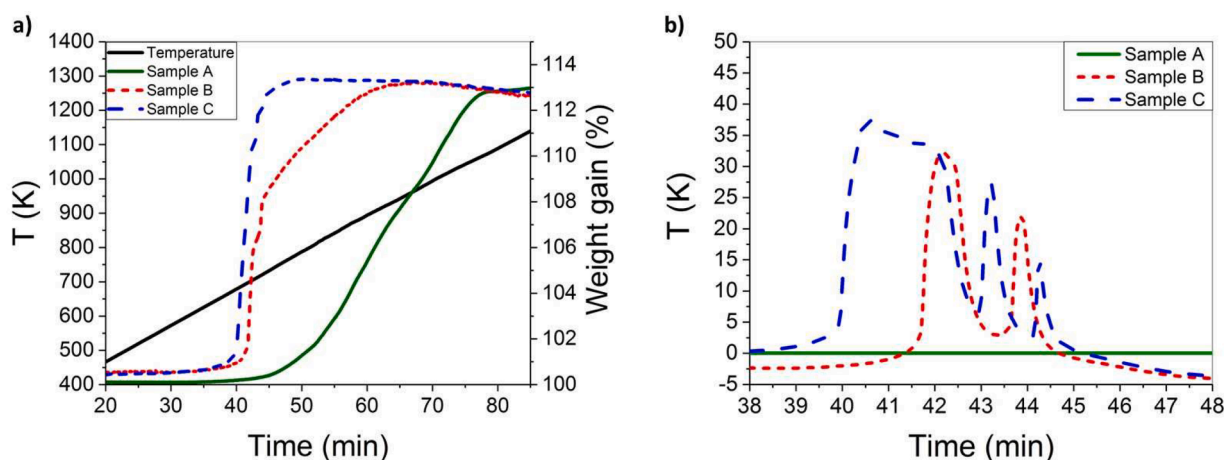


Fig. 5. a) Mass gain profile for samples A, B and C vs. temperature and time; b) Sample holder temperature increase during ignition of samples B and C.

from the temperature profile in the TGA/DSC or by visual inspection on samples tested in a HT-ESEM [23,24]. Fig. 7a shows the temperature at which ignition was triggered during the thermal ramp mode on UC fragments and in relation to the partial pressure of oxygen. Fig. 7b shows a plot of the time constant previously calculated in Gasparrini et al. [23]

on fragments tested in the HT-ESEM. The time constants, t_1 in Fig. 7b, represent the rate of cracks propagation (calculated as percentage of area covered by cracks) on the sample [23]. The methodology used to calculate t_1 is described in details in Gasparrini et al. [23], in summary, the trend of cracks propagation was observed to fit an exponential

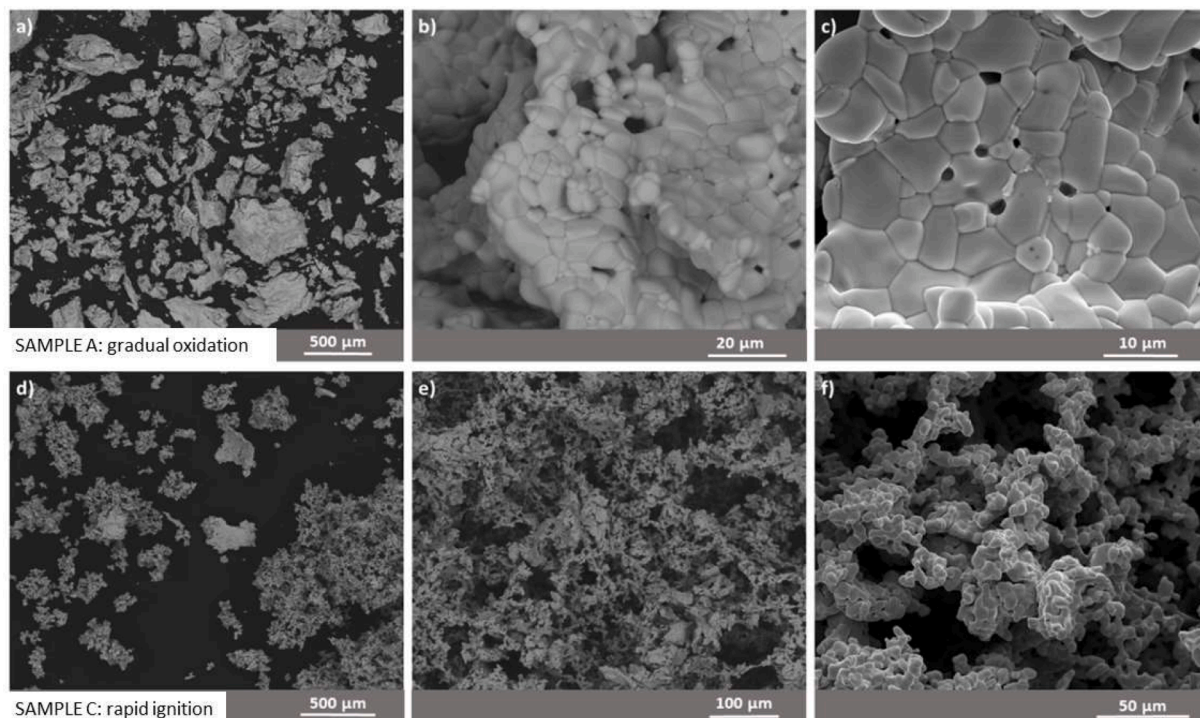


Fig. 6. BSEI (a, b, d and e) and SEI (c and f) of sample A (top row) and sample C (bottom row).

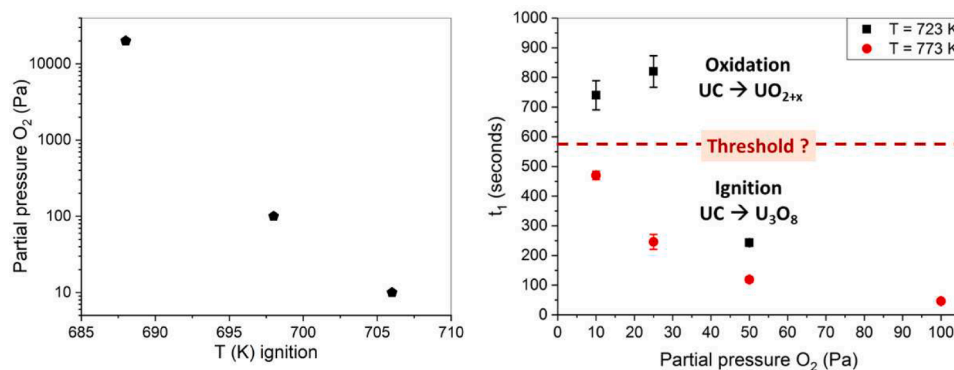


Fig. 7. a) Temperature at which UC ignition was triggered on fragments exposed to a thermal ramp mode at various oxygen partial pressure, b) Time constants t_1 (seconds) evaluated on area% plotted against oxygen partial pressure of UC samples oxidised at 723 K and 773 K in isothermal mode [23]: above the threshold UC ignition was not triggered, samples simply oxidised.

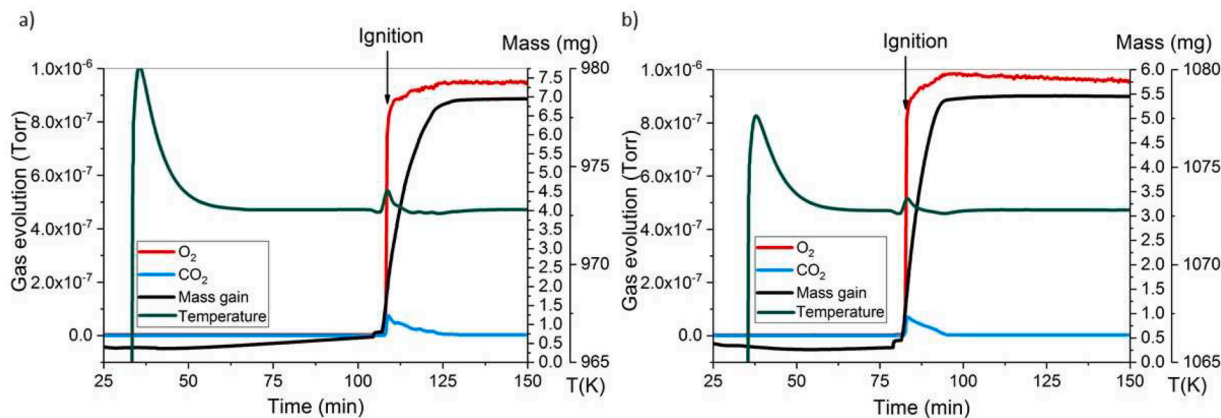


Fig. 8. TGA/DTA-MS data for fragments chosen from air-stored UC pellet oxidised in air at 973 (a) and 1073 K (b). The sharp temperature increase and steep mass increase are characteristics of ignition.

growth curve on all samples that underwent self-ignition, the curve was described with this Equation:

$$y = A \exp(x / t_1) \quad (2)$$

where A is a positive growth factor and t_1 is the time constant which represents the time t required for the function y , which is either the area % or cracks%, to increase by one factor Equal to e (see Fig. 5 in [23]). Time constants t_1 on samples that did not self-ignite but gradually oxidised instead were measured by plotting the natural logarithm of the normalised area% vs. time and by linearly fitting the initial part of the curve, after the induction time (see Fig. 8 in [23]). In this case the time constant t_1 is the inverse of the slope of the straight line, using Equation:

$$\ln(y) = \ln(A) + 1 / t_1 x \quad (3)$$

The samples that did not self-ignite gradually oxidised up to the UO_{2+x} stage. Fig. 7 summarises experiments conducted in isothermal mode in a HT-ESEM where UC fragments were exposed to several oxygen partial pressures and different temperatures. It can be observed that it is plausible that a t_1 threshold (calculated considering area%) exists between 470 and 740 s that characterise the behaviour of UC at low partial pressure of oxygen. A t_1 lower than the threshold (so far it was demonstrated for $t_1 < 470 \pm 14$ s) implies self-ignition, higher than the threshold (so far it was demonstrated for $t_1 > 740 \pm 49$ s) implies a slow and gradual oxidation to UO_{2+x} . Tests where self-ignition was not observed were conducted up to 723 K but at low oxygen partial pressures (10 and 25 Pa O_2).

Competition between cracking, which induced sample fragmentation, and oxide sintering is key to differentiate between oxidation and ignition mechanisms. Previous studies on UC oxidation stated that

oxidation to U_3O_8 could occur only after carbon transforms into CO and/or CO_2 [39]. Carbon in the form of thin graphite lamellae were detected in the oxide layers of UC powders exposed to oxygen at 473 K in Berthier et al. [40]

The one step reaction, UC to U_3O_8 , is considered the only reaction linked to UC ignition. To understand the gas release during this reaction, the evolution of gases during this stage was obtained in a TGA/DTA – MS experiment on fragments oxidised at 973 K and 1073 K. Gas evolution was monitored with time and cross-correlated to mass gain measurements. The evolution of CO_2 is shown in Fig. 8 for UC air-stored fragments. CO_2 was released as soon as oxygen was introduced to the chamber, as shown by the gas evolution in Fig. 8. Ignition was triggered by the exposure to oxygen in both samples (49.45 mg for 973 K and 39.61 mg for 1073 K), as seen from the sharp increase in the temperature profile and by the steep mass increase.

CO_2 is released at the same time as UC reacts with oxygen, forming U_3O_8 during ignition. To avoid overloading the crucible with oxide powder, the TGA/DTA – MS Equipment used for these experiments allowed for test samples with a maximum mass of 70 mg. All samples tested at 973 K and 1073 K underwent ignition, it was therefore impossible to monitor whether CO_2 was released during the first step of the reaction, when UC oxidises to UO_{2+x} prior to U_3O_8 . Ignition of UC was characterised in the TGA/DTA through the detection of a sudden temperature jump of the sample crucible and a sharp increase in the heat release. No temperature increase was detected in the sample holder when ZrC fragments were tested in air in ramp experiments up to 1673 K. This was also the case for isothermal oxidation tests on ZrC at 1073 K, 1173 K, 1273 K and 1373 K in air [27].

A comparison between weight gain and heat output of ZrC and UC fragments exposed at 1073 K to air using the same TGA/DTA

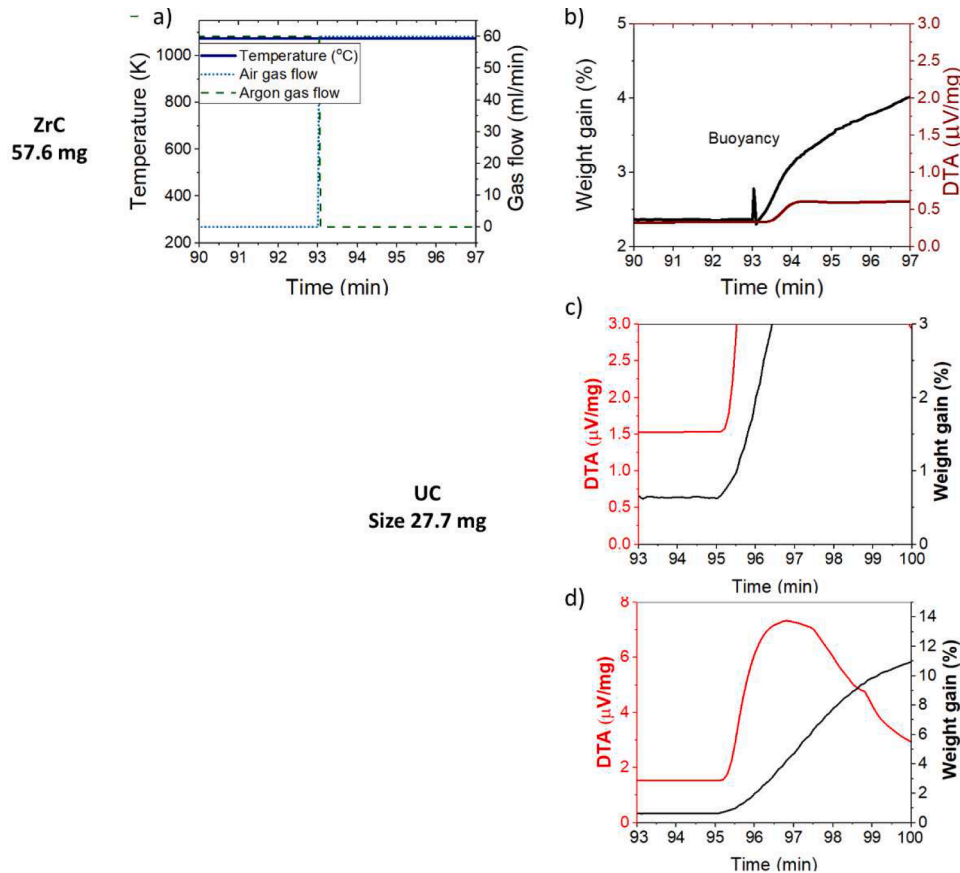
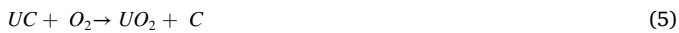


Fig. 9. TGA/DTA profiles of experiments performed on ZrC (the run shown used a 57.6 mg sample) and UC (the run shown used a 27.7 mg sample). Plot of gas flows switch between inert atmosphere and air (a); weight gain and heat output ($\mu V/mg$) of ZrC sample (b); weight gain and heat output ($\mu V/mg$) of UC sample plotted using the same scale as shown in (b) (c); weight gain and heat output ($\mu V/mg$) of UC sample extending both scales to show the full DTA peak.

experimental conditions is shown in Fig. 9.

As can be observed in Fig. 9, the reactivity of UC is much larger and much faster than ZrC (weight gain and heat output go beyond scale, see Fig. 9c).

UC ignition in air was related to a large enthalpy of reaction to U_3O_8 , estimated to be -1487 kJ/mol [15,41] at 298.15 K, according to Eq. 1. ZrC was never observed to ignite in air and the enthalpy of the ZrC to ZrO_2 reaction is -900 kJ/mol at 298.15 K (considering an enthalpy of formation for ZrC of -196.65 kJ/mol [42] and -1097.46 kJ/mol [42] for ZrO_2), according to Eq. 4. By applying the same method it is possible to demonstrate that the enthalpy of the reaction for ZrO_2 , -900 kJ/mol, is similar to that for the UC to UO_2 reaction, calculated to be -987 kJ/mol at 298.15 K according to Eq. 5. UC reacting to produce UO_2 and CO_2 according to Eq. 6 has an enthalpy of reaction of -1381.5 kJ/mol at 298.15 K. The reactions considered are:



UC oxidation to UO_2 is not considered to undergo ignition, as ZrC does not undergo ignition to ZrO_2 following Eq. (4). This is an important point to consider when large quantities of UC need to be conditioned into a stable oxide form for waste disposal: even though oxidation of UC to U_3O_8 in air is more convenient (furnaces are kept in air with no gas control), the fire risk from UC self-ignition cannot be excluded. Processing UC into UO_2 , instead, is a more complex process to conduct at scale but it should preclude the possibility of UC self-ignition and therefore fire.

Regarding further similarities between UC oxidation and ZrC

oxidation, special attention must be given to the role of carbon. Carbon has been quantified in the oxide formed from oxidation of UC [24] and ZrC [35]. A reason for the larger quantity of carbon in ZrO_2 produced at high temperature ($T = 1273$ K and 1373 K) compared to low temperatures ($T = 1073$ K and 1173 K) was related to the rapid oxide growth. The oxide produced was voluminous and the oxide growth rate was rapid at 1273 K and 1373 K. For carbon dispersed as inclusions in the oxide, or for the evolved CO/CO_2 , it would be expected that more difficulties would be encountered when escaping the system as the oxide grew thicker [35]. Another hypothesis was related to the fact that, at high temperatures (1273 K and 1373 K) zirconium oxidation is favoured than carbon oxidation. In this case, carbon liberated from the reaction of ZrC with oxygen remained embedded within the oxide with no possibility of reacting with oxygen, as zirconium would act as an oxygen getter, reacting first. This is at odds, however, with what was reported by Katoh et al. [26], who suggested that the carbon oxidation rate increased with the increase in temperature. A schematic that represents the hypotheses discussed is shown in Fig. 10.

If the mechanism for carbon oxidation proposed by Katoh et al. [26] for ZrC is correct: the oxidation rate of carbon should increase with temperature, fewer carbon inclusions should be expected in the ZrO_2 oxide formed in high temperature (1273 K) ZrC oxidation. This is the opposite of what was experimentally quantified in this work for ZrC since more residual carbon was measured in the ZrO_2 oxide at increased temperature. On the contrary, lower residual carbon was detected in U_3O_8 from UC oxidation at increased temperature. Carbon has been identified in the form of thin graphite lamellae retained in the oxide layers (UO_2) during UC powder oxidation below 503 K [40].

One of the reasons for the different trend of residual carbon in the oxides formed from the oxidation of UC and ZrC could be related to the different reactivity of the oxide itself with residual carbon/graphite. It

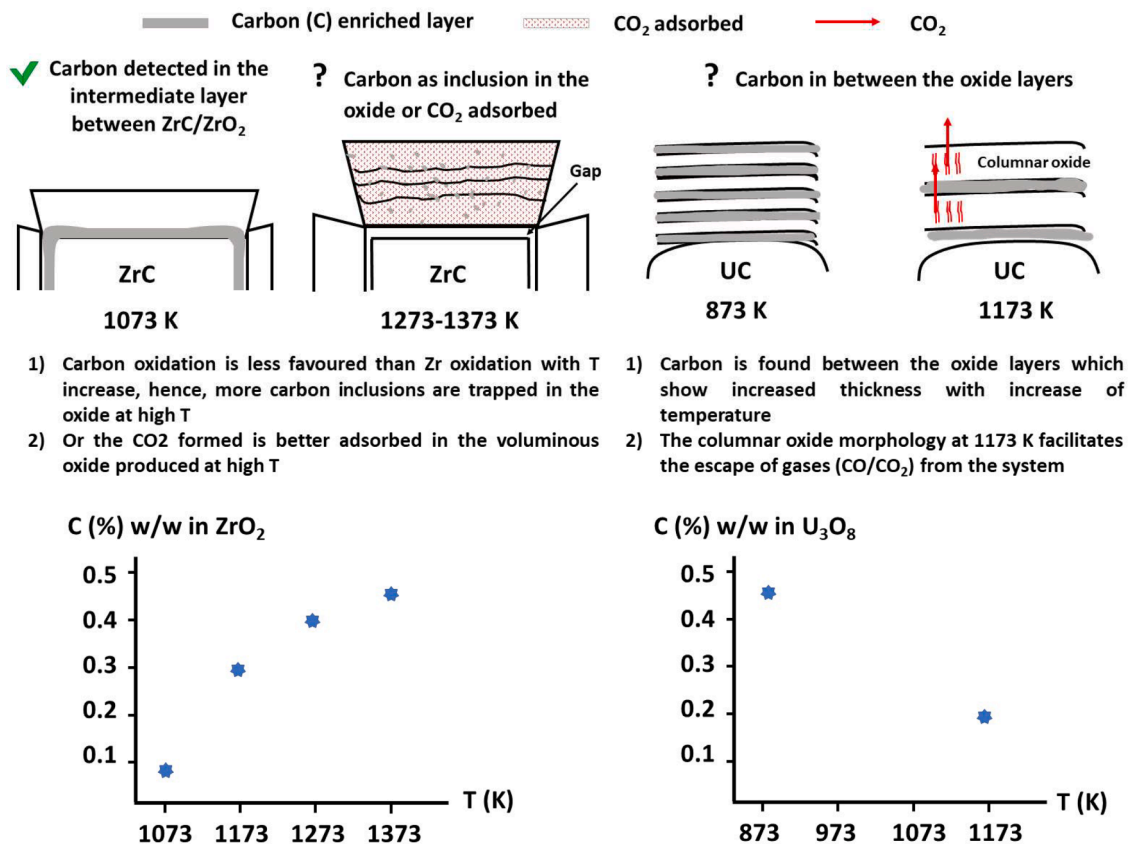


Fig. 10. Schematic that shows the fate of carbon or CO_2 in the oxide formed from oxidation of ZrC and UC in air (amorphous carbon was characterised in the intermediate layer between ZrC/ ZrO_2 [29] in samples oxidised at 1073 K with transmission electron microscopy). Note the opposite trend between carbon concentration and temperature in oxide formed in UC or ZrC oxidations.

was reported that U_3O_8 may act as a catalyst in the oxidation of graphite, or when in contact with carbon [43,44], adding a pathway for carbon oxidation to CO/CO_2 . One of the possibilities which could explain the results obtained on zirconia could be related to the CO_2 adsorption capability on m- ZrO_2 (given that carbon was measured with a technique that cannot distinguish between solid carbon or CO_2 gas [27]). The much voluminous and porous morphology of the oxide forms at higher temperature is observed visually, though, this hypothesis should be tested, by measuring the specific surface area of the oxides formed at different temperatures coupled with carbon analyses performed before and after degassing of samples to ensure that any carbon measured is adsorbed CO_2 .

4. Discussions

UC pyrophoricity is a process that needs to be better understood to limit potential hazards during nuclear fuel handling and prior to its safe disposal. Here it was shown that heat release from UC fragments was not affected by storage atmosphere (air vs inert atmosphere) during the three months period of testing on UC samples that already contained a UO_2 phase. Ignition released the same amount of heat from fragments no matter if they were produced and stored in an air atmosphere or an inert atmosphere. Ignition of UC disrupted the U_3O_8 morphology of the oxide and the reaction was characterised by a sharp increase in mass and a sharp heat release, coupled with an increase of temperature of the structure surrounding the sample (i.e. the TGA sample holder as shown in Fig. 5b). An additional information was the role of cracking in the oxide in relation to ignition or oxidation. A very approximate approach to estimate stresses in the oxide is discussed in the following section to explain the link with cracking of the oxide.

4.1. Stresses in the oxide inducing cracks

Oxidation of ZrC [29,35] and UC [24] are influenced by crack formation and propagation. UC ignition initiation, for example, was triggered by sample fragmentation induced by a network of cracks [23]. One of the driving forces for crack formation is relaxation of tensile stresses. Hence, the cracking and sample fragmentation observed in both ZrC and UC oxides could be related to stresses in the carbide/oxide system. Using a very simplistic methodology and approximation, stresses generated during oxidation of UC were calculated in Gasparrini et al. [24] to be 34–52 GPa for the oxidation of UC to UO_2 and 52 GPa for UO_2 to U_3O_8 . Using the same approach [45], here these stresses generated during oxidation ZrC to the oxide, ZrO_2 are reported and compared to those generated during UC oxidation. The stresses in the oxide layer were considered to be primarily induced by a mismatch between crystal structures. In order to give a rough estimate of the stresses present in the oxide layer, the system was considered as being comprised of two layers: a carbide layer and an oxide sitting on top. Since the carbide samples considered in this study are all polycrystalline materials, we expect different crystal orientations for the oxide to grow on top of the carbide

grain. The oxide crystal structure was simplified and considered cubic and isotropic. To calculate the residual stresses in the oxide layer the Equation from Wang et al. [46] was used. This same method was used to evaluate the approximate strain and stresses between the carbide and the oxide in the ZrC/ ZrO_2 and UC/ UO_2 / U_3O_8 systems. The lattice spacing of the stressed oxide layer, d in Eq. (7), was taken from the tabulated value of the carbide, as if the oxide was constrained to mimic the carbide crystal structure. The value for the lattice spacing of the stress-free oxide layer, d_0 , was taken from the tabulated value of the oxide, as if it was free from constraints. A schematic of the model considered is shown in Fig. 11b.

The isotropic strain ε , representative of all directions in the crystal, was linked to an approximate d spacing, here called d^* , calculated from the data of the volume cell, V using this Equation:

$$d^* = \sqrt[3]{V} \quad (7)$$

where V is the volume cell normalised per Z and per metal atom. ε was calculated with Equations presented in Gasparrini et al. [24] using the d^* values, where d is substituted with d^* of the carbide and d_0 with d^* of the oxide. The stress, σ , was calculated using Equations in Gasparrini et al. [24] knowing the Young's modulus, E , and Poisson's ratio, ν , for the oxide considered. The compressive stresses of the oxides, in both ZrC and UC, are shown in Table 2.

Stresses and strains calculated in Table 2 are approximated as these were calculated using several assumptions (for example the system considered was ideal and isotropic). An indication of the reliability of these values is given by Ahn [51] who studied fracture stresses caused by UO_2 oxidation during dry storage of spent fuels. The similar order of magnitude between the stress values reported by Ahn [51] and the values presented here give an indication of the large forces and stresses occurring during carbide oxidation. In Ahn's work [51] the large volume expansion and resultant stress involved in the transformation from UO_2 to U_3O_8 was identified as the underlying cause of the pulverisation mechanism observed when UO_2 oxidises to U_3O_8 . In this case, the morphology of the oxide changes completely into a powder, this transformation is commonly called popcorn-like [55]. The ignition mechanism of UC shows the largest value of stress in Table 2, approximately 98 GPa. The presence of such a large stress in the oxide layer may well explain the sudden explosive transformation monitored during ignition. In the ZrC system, the reaction presenting the lowest stress in the oxide is the formation of t- ZrO_2 rather than m- ZrO_2 (40 versus 55 GPa respectively, at $T = 1273$ K). Data for E and ν of pure c- ZrO_2 could not be found in the literature, as it is a high temperature stabilised phase. However, values for an yttria-cubic stabilised zirconia (Y-CSZ), stabilised at room temperature, was found and reported in Table 2. The stress experienced during the transformation from ZrC to Y-CSZ was 47 GPa, larger than the one calculated for t- ZrO_2 , but smaller than the one calculated for m- ZrO_2 . The t/c- ZrO_2 polymorphs were observed at temperatures below their phase stability ranges as they were responsible for the first step of the oxidation mechanism of ZrC [35]. The formation of these polymorphs instead of m- ZrO_2 , expected to be the most stable polymorph at

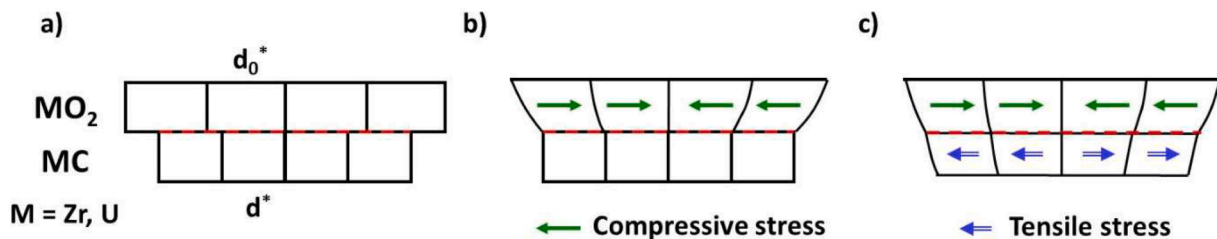


Fig. 11. Schematic of the system considered for approximate strain and stress analysis, the effect of the intermediate layer between carbide and oxide (highlighted with a dashed red line) was not considered: a) ideal system where the oxide layer does not show any epitaxial relations to the carbide, b) system used for strain and stress calculations: the oxide layer is constrained to assume the structure of the carbide layer, c) both the carbide and oxide layers show stresses induced by epitaxial growth (this is closer to reality but difficult to obtain information from).

Table 2

Values of approximate d spacing, strain and stresses in the oxide layers (Y-CSZ stands for yttria-cubic stabilised zirconia).

Species	Z	V/Z per metal (\AA^3)	d* (\AA)	E (GPa)	ν	Reaction	ε	σ (GPa)	Ref. (E, ν)
ZrC	4	25.807	2.955						
m-ZrO ₂	4	35.165	3.276	241	0.3	ZrC \rightarrow m-ZrO ₂	-0.098	-59.05	[47,48]
				226 ($T = 1273$ K)				-55.37	
t-ZrO ₂	2	33.355	3.219	195.5 ($T = 1273$ K)	0.3	ZrC \rightarrow t-ZrO ₂	-0.082	-40.08	[47,48]
c-ZrO ₂	4	33.713	3.23	-	-	ZrC \rightarrow c-ZrO ₂	-0.085	-	[49,50]
Y-CSZ				222	0.3			-47.18	
UC	4	30.45	3.123						
UO ₂	4	40.85	3.444	145	0.302	UC \rightarrow UO ₂	-0.094	-34.42	[51,52]
U ₃ O ₈	2	55.516	3.815	151	0.36*	UO ₂ \rightarrow U ₃ O ₈	-0.097	-52.31	[53,54]
						UC \rightarrow U ₃ O ₈	-0.181	-97.61	[53,54]

The ν (*) value for U₃O₈ is an average measured from the values reported by Szpunar & Szpunar [54]: 0.66 reported along [100], [010] and 0.06 along [001] directions due to the large anisotropy of U₃O₈.

the temperatures considered, can here be related to a stress minimisation effect.

4.2. Presence of unreacted carbon in the oxide layer

Carbon, or bonded carbon, was present in the oxide layer from the oxidation of ZrC and UC. It is still unclear in which form carbon occurs in the oxide and what the underlying mechanism for its formation is. The carbon content of the oxide increased with oxidation temperature for ZrC while it decreased with oxidation temperature for UC. The presence of carbon may be related to how the oxide cracks and the oxide morphology. The form of carbon in the oxide is not clear due to limitations in the experimental technique used in its quantification (the elemental analysis performed was unable to differentiate between bonded carbon or free carbon, as it only measures the amount of CO/CO₂ from combustion). Carbon measured within the oxide could be in the form of amorphous carbon, carbide, oxycarbide or as CO/CO₂ produced during oxidation. The adsorption of CO₂ in zirconia has been studied [56,57,58]: the CO₂ adsorption capacity of m-ZrO₂ is one order of magnitude higher than that of t-ZrO₂. The oxide formed during oxidation of ZrC at 1273 K and 1373 K was voluminous m-ZrO₂ in contrast with the compact m-ZrO₂ and t/c-ZrO₂ at 1073 K and 1173 K [35]. A larger concentration of CO₂ in the oxide at 1273 K and 1373 K could be linked to the capacity of the cracked and porous m-ZrO₂ to adsorb CO₂ better than the m-ZrO₂ and t/c-ZrO₂. CO₂ gas development is key in carbide oxidation, Holcomb et al. [59] proposed a counter-diffusion model that describes the fluxes of O₂ and CO₂ in and out of a sample during oxidation of HfC. UC showed a decreasing concentration of carbon with increasing temperature. At 873 K the oxide layer contained approximately 4700 ppm of carbon while at high temperature (1173 K) the oxide contained approximately 2000 ppm of carbon [24]. Carbon analyses for ZrC and UC were conducted on partially oxidised samples. When carbon analysis was performed on fully oxidised UC oxidised samples, carbon content decreased considerably. Carbon content was still larger at 873 K compared to the one detected at 1173 K, 470 ppm versus 327 ppm respectively [24].

The lower concentration of carbon in uranium oxide samples at higher temperatures, 1173 K versus 873 K, could be correlated to the morphology of the oxide layer. At 1173 K the oxide was thicker than the one formed at 873 K and underwent a sintering process due to an increase in plasticity of the oxide, U₃O₈. Columnar grains were observed in the oxide at 1173 K while at 873 K the oxide was in a powdered form [24]. The columnar grain morphology of the oxide at high temperature, 1173 K, could explain why the amount of carbon remaining in the oxide formed is lower than in the oxide formed at 873 K. A columnar morphology in the oxide layer could help the evolved CO₂ gas easily escape the system [24]. Such columnar morphology was shown to be a favourable route for voids or for vapour-phase transport [60]. The ease by which carbon could leave the system as CO/CO₂ would translate into a lower amount of carbon dispersed as an inclusion in the oxide layer, in

line with experimental evidence. Another possible explanation for the lower amount of carbon at 1173 K than at 873 K could be related to the thickness of the oxide layers. If it is assumed that UC and ZrC follow the same oxidation mechanism, then, if the carbon in the oxide was amorphous carbon at the interface carbide/oxide, as for ZrC, less carbon would be found in the sample volume at 1173 K compared to 873 K because thinner oxide layers were observed hence more interface carbide/oxide are present.

It should be noted that the same amount of carbon was observed on oxide layers from samples oxidised at the same temperature but for two different exposure times, at 1273 K for 30 min and 8 h for ZrC. In UC, carbon analysis was performed on samples oxidised at 873 K and 1173 K for 6 h dwell time but kept in the furnace for different times: 17.5 and 22 h because sample quenching was not practicable due to possible presence of pyrophoric unreacted UC in the oxide. The reason for the carbon decrease as temperature increased in U₃O₈ may be due to the different times spent inside the furnace. It is worth noting though that in ZrO₂ the oxidising time did not influence carbon content. UC can undergo ignition and this reaction directly produced CO₂ (as shown in Fig. 8) instead of free carbon, C [15]. This could influence the presence of carbon in the oxide. The correlation between sample ignition and carbon content should be investigated further, as well as coupling a CO₂ gas analyser during small scale furnace tests to correlate the amount of CO₂ with carbon left in the oxide.

5. Conclusions

UC pyrophoricity and oxidation of ZrC and UC were investigated experimentally coupling multiple techniques at a hierarchical level of analysis: from macrostructural to nanostructural characterisation through the implementation of state-of-the-art techniques. The main findings are now listed:

- Heat release from UC oxidation experiments was tested on fragments that were stored for 3 months in either air or an inert atmosphere. UC fragments were manufactured from legacy fuels stored in air for decades, UO₂ phase was detected. Fragments stored in both atmospheres did not show differences when measuring the heat release during ignition.
- Pyrophoricity was confirmed to depend on temperature and partial pressure: UC pyrophoricity was not triggered when fragments were exposed to high temperatures, 723 K, and low oxygen partial pressures, 10 and 25 Pa in a HT-ESEM
- Carbon (in the form of amorphous carbon, carbide or CO/CO₂) was detected in the oxide due to oxidation of ZrC and UC. Residual carbon in the oxide after ZrC oxidation from 1073 K to 1373 K increased in ZrO₂ whilst it decreased with temperature in U₃O₈ after oxidation of UC from 873 K to 1173 K.
- Oxide cracking in both ZrC and UC oxidation was here ascribed to stresses generated from the volumetric transformations from the

carbide to the oxide. Enthalpy of reaction and stresses in the oxide layer were maximum for the ignition reaction that occurs from UC to U_3O_8 were largest stresses in the oxide were estimated.

CRedit authorship contribution statement

C. Gasparrini: Conceptualization, Formal analysis, Investigation, Visualization, Writing – original draft. **R. Podor:** Investigation, Conceptualization, Resources, Writing – review & editing. **O. Fiquet:** Resources, Validation, Writing – review & editing. **M.J.D. Rushton:** Conceptualization, Writing – review & editing. **W.E. Lee:** Writing – review & editing, Supervision, Funding acquisition.

Declaration of competing interest

The authors declare that they have no known competing financial interests or personal relationships that could have appeared to influence the work reported in this paper.

Acknowledgements

The authors are grateful to the EPSRC DISTINCTIVE (Decommissioning, Immobilization and Storage solutions for Nuclear waste Inventories) Consortium for their financial support of this project (EPSRC Industrial Case Award EP/M507428/1 Grant and the DISTINCTIVE EP/L014041/1 Grant). We also thank collaborators at the National Nuclear Laboratory, building A709, Preston, UK: Sarah May, Peter Durham, Simon Overall, Dr. Daniel Shepherd and Dr. Duncan Coppersthaite.

References

- INTERNATIONAL ATOMIC ENERGY AGENCY, Advanced fuel technology and performance: Current status and trends, IAEA-TECDOC-577, Proceedings of an Advisory Group Meeting, organised by International Atomic Energy Agency, Vienna 27–29 November 1989 (1990).
- INTERNATIONAL ATOMIC ENERGY AGENCY, "Accident tolerant fuel concepts for light water reactors" IAEA-TECDOC-1797 Proceedings of a Technical Meeting held at Oak Ridge National Laboratories, United States of America, 13–16 October 2014 (2016).
- J.D. Hales, K.A. Gamble, Modelling advanced technology fuels, enlarged Halden group meeting 2017, 2017. INL/CON-17-42151 Prepr.
- S.J. Zinkle, K.A. Terrani, J.C. Gehin, L.J. Ott, L.L. Snead, Accident tolerant fuels for LWRs: a perspective, *J. Nucl. Mater.* 448 (1–3) (2014) 374–379.
- P. Hosemann, D. Frazer, M. Fratoni, A. Bolind, M.F. Ashby, Materials selection for nuclear applications: challenges and opportunities, *Scr. Mater.* 143 (2018) 181–187.
- D. Manara, F. De Bruycker, A.K. Sengupta, R. Agarwal, and H.S. Kamath, "Thermodynamic and thermophysical properties of the actinide carbides," in Section 2.04 in Comprehensive Nuclear Materials – Volume 2, 2012, pp. 89–149.
- M. Kurata, Research and development methodology for practical use of accident tolerant fuel in light water reactors, *Nucl. Eng. Technol.* 48 (1) (2016) 26–32.
- J.K. Watkins, A.R. Wagner, A. Gonzales, B.J. Jaques, E.S. Sooby, Challenges and opportunities to alloyed and composite fuel architectures to mitigate high uranium density fuel oxidation: uranium diboride and uranium carbide, *J. Nucl. Mater.* 560 (2022) 153502.
- A. Gonzales, J.K. Watkins, A.R. Wagner, B.J. Jaques, E.S. Sooby, Challenges and opportunities to alloyed and composite fuel architectures to mitigate high uranium density fuel oxidation: uranium silicide, *J. Nucl. Mater.* 553 (2021) 153026.
- J.K. Watkins, A. Gonzales, A.R. Wagner, E.S. Sooby, B.J. Jaques, Challenges and opportunities to alloyed and composite fuel architectures to mitigate high uranium density fuel oxidation: uranium mononitride, *J. Nucl. Mater.* 553 (2021) 153048.
- S.K. Borowski, D.R. McCurdy, T.W. Packard, Nuclear thermal rocket/vehicle characteristics and sensitivity trades for NASA's Mars design reference architecture (DRA) 5.0 study, *Proc. Nucl. Emerg. Technol. Sp* (2009) no. Paper 203599.
- V.A. Eliseev, L.M. Zaboudko, I.V. Malysheva, V.I. Matveev, Nitride fuel for a prospective BN-1200 type fast sodium reactor, *Energy* 114 (5) (2013) 331–336.
- Nuclear Decommissioning Authority, "Exotic fuels and nuclear materials –Dounreay –Credible options –Final Document Ref SMS/TS/B&C3/NM&EF/001/A," no. February 2012.
- C. Duguay, G. Pelloquin, Fabrication of mixed uranium–plutonium carbide fuel pellets with a low oxygen content and an open-pore microstructure, *J. Eur. Ceram. Soc.* 35 (14) (2015) 3977–3984.
- M. Dell, V.J. Wheeler, The ignition of uranium mononitride and uranium monocarbide in oxygen, *J. Nucl. Mater.* 21 (1967) 328–336.
- C. Berthier, S. Coullomb, C. Rado, E. Blanquet, R. Boichot, C. Chatillon, Experimental study of uranium carbide pyrophoricity, *Powder Technol.* 208 (2) (2011) 312–317.
- Nuclear Decommissioning Authority, "Exotic fuels and nuclear materials –Dounreay –Preferred options (Gate B). Document Reference: SMS/TS/B&C3/NM&EF/001/B," no. February 2013.
- M. Paljević, Z. Despotović, Oxidation of uranium mononitride, *J. Nucl. Mater.* 57 (3) (1975) 253–257.
- E. Sooby Wood, J.T. White, A.T. Nelson, Oxidation behavior of U-Si compounds in air from 25 to 1000 °C, *J. Nucl. Mater.* 484 (2017) 245–257.
- E.S. Wood, J.T. White, C.J. Grote, A.T. Nelson, U_3Si_2 behavior in H_2O : part I, flowing steam and the effect of hydrogen, *J. Nucl. Mater.* 501 (2018) 404–412.
- R.W. Harrison, C. Gasparrini, R.N. Worth, J. Buckley, M.R. Wenman, T. Abram, On the oxidation mechanism of U_3Si_2 accident tolerant nuclear fuel, *Corros. Sci.* 174 (June) (2020) 108822.
- F. Le Guyader, C. Rado, S. Joffe, S. Coullomb, C. Chatillon, E. Blanquet, Thermodynamic and experimental study of UC powders ignition, *J. Nucl. Mater.* 393 (2) (2009) 333–342.
- C. Gasparrini, R. Podor, D. Horlait, M.J.D. Rushton, O. Fiquet, W.E. Lee, Oxidation of UC: an *in situ* high temperature environmental scanning electron microscopy study, *J. Nucl. Mater.* 494 (2017) 127–137.
- C. Gasparrini, et al., Uranium carbide oxidation from 873K to 1173K, *Corros. Sci.* 151 (2019) 44–56.
- L.E. Musgrave, A theory of burning curve ignition of nuclear metals, *J. Nucl. Mater.* 43 (2) (1972) 155–163.
- Y. Katoh, G. Vasudevamurthy, T. Nozawa, L.L. Snead, Properties of zirconium carbide for nuclear fuel applications, *J. Nucl. Mater.* 441 (1–3) (2013) 718–742.
- C. Gasparrini, et al., On the stoichiometry of zirconium carbide, *Sci. Rep.* 10 (1) (2020) 6347.
- B. Panda, S. Shah, and R.R. Hickman, "Solid solution carbides are the key fuels for future nuclear thermal propulsion," 2005.
- C. Gasparrini, R. Podor, D. Horlait, R. Chater, W.E. Lee, Zirconium carbide oxidation: maltese cross formation and interface characterization, *Oxid. Met.* 88 (3–4) (2017) 509–519.
- J. Besson, C. Moureau, La réaction de l'oxygène sur le monocarbure d'uranium massif, *Compt. Rend. Acad. Sci. Paris*, vol. 258 (1964) 4079–4082.
- D. Mattia, M. Desmaison-Brut, S. Dimovski, Y. Gogotsi, J. Desmaison, Oxidation behaviour of an aluminium nitride-hafnium diboride ceramic composite, *J. Eur. Ceram. Soc.* 25 (10) (2005) 1789–1796.
- S.C. Cifuentes, M.A. Monge, P. Pérez, On the oxidation mechanism of pure tungsten in the temperature range 600–800 °C, *Corros. Sci.* 57 (2012) 114–121.
- Nuclear Decommissioning Authority, "Uranics: credible Options Summary (Gate A). Doc Ref: SMS/TS/B2-UR/002/A v1.0," no. January, pp. 1–11, 2014.
- G. Raveu, "Optimisation de la fabrication par carbothermie de carbure d'uranium à teneur en oxygène maîtrisée," Thèse Dr. en Phys. des matériaux des surfaces-Sous la Dir. Marie-France Barthe. École Dr. Énergie, Matériaux, Sci. la Terre l'Univers (Centre-Val Loire), p. 282, 2014.
- C. Gasparrini, R.J. Chater, D. Horlait, L. Vandeperre, W.E. Lee, Zirconium carbide oxidation: kinetics and oxygen diffusion through the intermediate layer, *J. Am. Ceram. Soc.* 101 (6) (2018) 2638–2652.
- R.E. Rundle, N.C. Baenziger, A.S. Wilson, R.A. McDonald, The structures of the carbides, nitrides and oxides of uranium, *J. Am. Chem. Soc.* 70 (55) (1948) 99–105.
- A.E. Austin, Carbon positions in uranium carbides, *Acta Crystallogr.* 12 (2) (1959) 159–161.
- R. Fritsche and C. Sussieck-Fornefeld, "ICDD Grant-in-Aid, Min.- Petr. Inst., Univ., Heidelberg, Germany." 1988.
- V.S. Iyer, et al., Oxidation behavior of carbide fuels, *Nucl. Technol.* 91 (1990) 388–393.
- C. Berthier, et al., Experimental kinetic study of oxidation of uranium monocarbide powders under controlled oxygen partial pressures below 230 °C, *J. Nucl. Mater.* 432 (1–3) (2013) 505–519.
- R.J.M. Konings, L.R. Morss, J. Fuger, Thermodynamic properties of actinides and actinide compounds. The Chemistry of the Actinide and Transactinide Elements, Springer, 2006, pp. 2113–2224.
- R.W. Harrison, W.E. Lee, Processing and properties of ZrC, ZrN and ZrCN ceramics: a review, *Adv. Appl. Ceram.* 115 (5) (2016) 294–307.
- S. Sampath, N.K. Kulkarni, D.M. Chackraburtty, Influence of selected metal oxides on the oxidation kinetics of graphite, *Thermochim. Acta* 86 (C) (1985) 7–15.
- D.W. McKee, Rare earth oxides as carbon oxidation catalysts, *Carbon N. Y.* 23 (6) (1985) 707–713.
- C. Gasparrini, Oxidation of Zirconium and Uranium Carbides, Department of Materials, Imperial College London, 2018. PhD Thesis.
- X.L. Wang, C.R. Hubbard, K.B. Alexander, P.F. Bech, Neutron diffraction measurements of the residual stresses in $Al_2O_3-ZrO_2(CeO_2)$ ceramic composites, *J. Am. Ceram. Soc.* 77 (6) (1994) 1569–1575.
- E.Y. Fogaing, Y. Lorgouilloux, M. Huger, C.P. Gault, Young's modulus of zirconia at high temperature, *J. Mater. Sci.* 41 (22) (2006) 7663–7666.
- R.H.J. Hannink, P.M. Kelly, B.C. Muddle, Transformation toughening in zirconia-containing ceramics, *J. Am. Ceram. Soc.* 83 (3) (2004) 461–487.
- J.W. Adams, R. Ruh, K.S. Mazdiyasi, Young's modulus, flexural strength, and fracture of yttria-stabilised zirconia versus temperature, *J. Am. Ceram. Soc.* 80 (4) (1997) 903–908.
- International Syalons, "Zircaloy 5 & Zircaloy 10 property data sheet," Mater. Prop. datasheet Int. Syalons, 2017.

- [51] T.M. Ahn, "Dry oxidation and fracture of LWR spent fuels," NUREG-1565, Div. Waste Manag. Off. Nucl. Mater. Saf. Safeguards, U.S. Nucl. Regul. Comm. Washington, DC 20555-0001, no. September 1996.
- [52] S.M. Lang, Properties of high-temperature ceramics and cermets: elasticity and density at room temperature," Monogr. 6, Natl. Bur. Stand. Washington D.C. (1960).
- [53] B. Szpunar, J.A. Szpunar, V. Milman, A. Goldberg, Implication of volume changes in uranium oxides: a density functional study, Solid State Sci. 24 (2013) 44–53.
- [54] B. Szpunar, J.A. Szpunar, Theoretical investigation of structural and mechanical properties of uranium oxide, in: Uranium 2010, Proceeding 3rd International Conference Uranium, Saskatoon, Saskatchewan, Canada, vol. 2, 2010, pp. 177–187.
- [55] R.J. McEachern, P. Taylor, A review of the oxidation of uranium dioxide at temperatures below 400°C, J. Nucl. Mater. 254 (2–3) (1998) 87–121.
- [56] B. Bachiller-Baeza, I. Rodriguez-Ramos, A. Guerrero-Ruiz, Interaction of carbon dioxide with the surface of zirconia polymorphs, Langmuir 14 (14) (1998) 3556–3564.
- [57] V. Hornebecq, C. Knöfel, P. Boulet, B. Kuchta, P.L. Llewellyn, Adsorption of carbon dioxide on mesoporous zirconia: microcalorimetric measurements, adsorption isotherm modeling, and density functional theory calculations, J. Phys. Chem. C 115 (20) (2011) 10097–10103.
- [58] K. Pokrovski, K.T. Jung, A.T. Bell, Investigation of CO and CO₂ adsorption on tetragonal and monoclinic zirconia, Langmuir 17 (14) (2001) 4297–4303.
- [59] G.R. Holcomb, G.R.S. Pierre, Application of a counter-current gaseous diffusion model to the oxidation of hafnium carbide at 1200 to 1530°C, Oxid. Met. 40 (1–2) (1993) 109–118.
- [60] F.A. Nichols, Transport phenomena in nuclear fuels under severe temperature gradients, J. Nucl. Mater. 84 (1–2) (1979) 1–25.